JOURNAL OF GEOPHYSICAL RESEARCH, VOL. 112, D15306, doi:10.1029/2006JD008355, 2007

Sounding of the Atmosphere using Broadband Emission Radiometry observations of daytime mesospheric $O_2(^1\Delta)$ 1.27 μm emission and derivation of ozone, atomic oxygen, and solar and chemical energy deposition rates

Martin G. Mlynczak,[1] B. Thomas Marshall,[2] F. Javier Martin-Torres,[3] James M. Russell III,[4] R. Earl Thompson,[2] Ellis E. Remsberg,[1] and Larry L. Gordley[2]

Received 15 December 2006; revised 19 April 2007; accepted 23 May 2007; published 11 August 2007.

[1] We report observations of the daytime $O_2(^1\Delta)$ airglow emission at 1.27 μm recorded by the Sounding of the Atmosphere using Broadband Emission Radiometry (SABER) instrument on the NASA Thermosphere-Ionosphere-Mesosphere Energetics and Dynamics (TIMED) satellite. The measured limb radiances are inverted to yield vertical profiles of the volume emission rate of energy from the O_2 molecule. From these emission rates we subsequently derive the mesospheric ozone concentrations using a nonlocal thermodynamic equilibrium (non-LTE) radiative and kinetic model. Rates of energy deposition due to absorption of ultraviolet radiation in the Hartley band of ozone are also derived, independent of knowledge of the ozone abundance and solar irradiances. Atomic oxygen concentrations are obtained from the ozone abundance using photochemical steady state assumptions. Rates of energy deposition due to exothermic chemical reactions are also derived. The data products illustrated here are from a test day (4 July 2002) of SABER Version 1.07 data which are now becoming publicly available. This test day illustrates the high quality of the SABER $O_2(^1\Delta)$ airglow and ozone data and the variety of fundamental science questions to which they can be applied.

Citation: Mlynczak, M. G., B. T. Marshall, F. J. Martin-Torres, J. M. Russell III, R. E. Thompson, E. E. Remsberg, and L. L. Gordley (2007), Sounding of the Atmosphere using Broadband Emission Radiometry observations of daytime mesospheric $O_2(^1\Delta)$ 1.27 μm emission and derivation of ozone, atomic oxygen, and solar and chemical energy deposition rates, *J. Geophys. Res.*, *112*, D15306, doi:10.1029/2006JD008355.

1. Introduction

[2] The daytime terrestrial $O_2(^1\Delta)$ airglow emission provides a fundamental probe into the photochemistry and energetics of the mesosphere and lower thermosphere. It has been observed frequently by rocket-borne instruments [e.g., *Evans et al.*, 1968; *Mlynczak et al.*, 2001] and from space by the Near-Infrared Spectrometer instrument on the Solar Mesospheric Explorer (SME) satellite [*Thomas et al.*, 1984] and by the Optical Spectrograph and InfraRed Imager System (OSIRIS) instrument on the Odin satellite [*Llewellyn et al.*, 2004]. $O_2(^1\Delta)$ is produced primarily by photolysis of ozone in the Hartley band and provides a strong and distinct radiative signal that is readily measured and used to infer the ozone concentration in the mesosphere. The $O_2(^1\Delta)$ emission also plays a fundamental role in the radiative energy balance of the mesosphere [e.g., *Mlynczak and Solomon*, 1991].

[3] The SABER instrument [*Russell et al.*, 1999] was launched on the NASA TIMED satellite in December 2001. A fundamental goal of SABER is to observe comprehensively the ozone abundance and energy balance of the terrestrial mesosphere [*Mlynczak*, 1997]. One of the key measurements toward achieving this goal is the global observations of the $O_2(^1\Delta)$ airglow emission at 1.27 μm. In this paper we outline the SABER observations of the $O_2(^1\Delta)$ airglow and the data products derived from it. The data presented here are based on the Version 1.07 processing which are now becoming publicly available. This new version updates the presently available Version 1.06 primarily in the blending of emission rates retrieved separately under the weak-line and strong-line radiative transfer regimes. The spectroscopy in the non-LTE kinetic model and in the strong-line retrieval algorithm has been updated in Version 1.07 to be consistent. These changes, while important in the overall data quality, are typically at the 10% level in the inferred ozone abundance from that presented in Version 1.06.

[4] In the following sections we describe the retrieval approaches and the data products derived from the airglow

[1] NASA Langley Research Center, Hampton, Virginia, USA.
[2] G&A Technical Software, Newport News, Virginia, USA.
[3] Analytical Services and Materials, Inc., Hampton, Virginia, USA.
[4] Department of Atmospheric and Planetary Sciences, Hampton University, Hampton, Virginia, USA.

0148-0227/07/2006JD008355$09.00

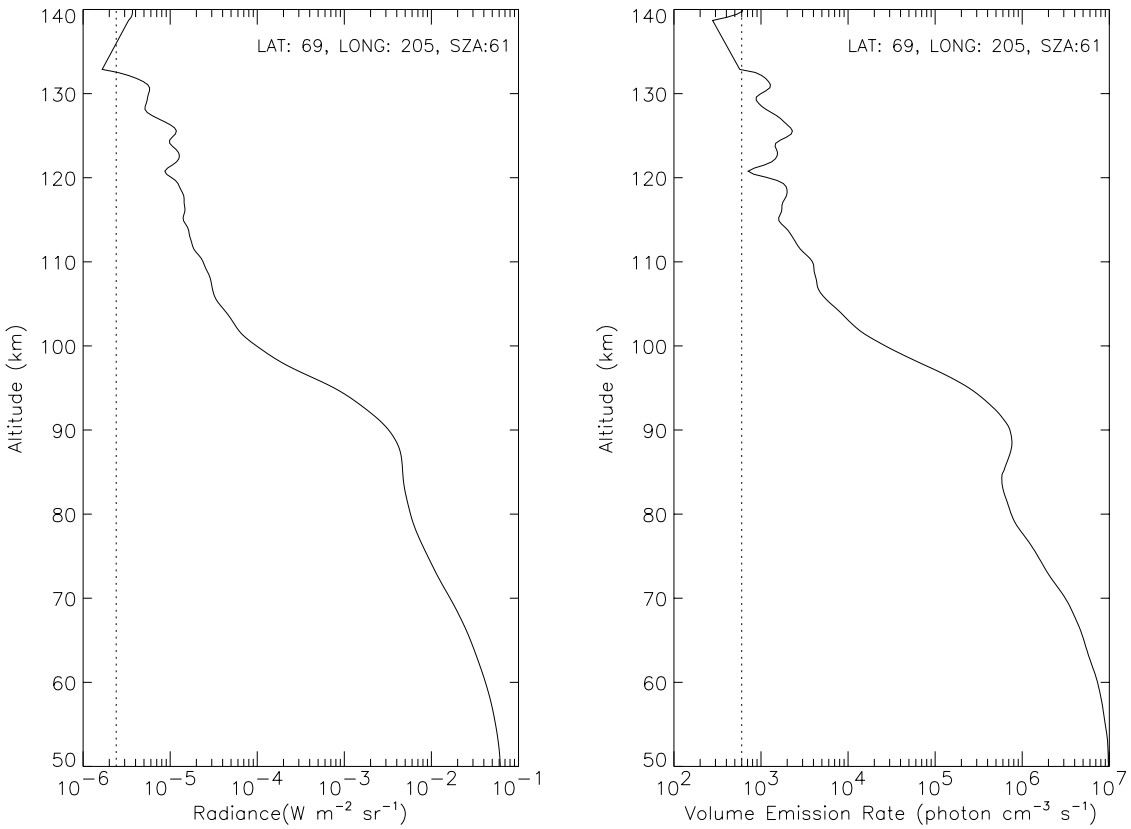

Figure 1. SABER $O_2(^1\Delta)$ (left) limb radiance and (right) retrieved volume emission rate of photons at 69°N, 205°W, with solar zenith angle of 61°, 4 July 2002. Noise levels are given by the individual vertical dotted lines. Note that the signal-to-noise ratio exceeds 1000 below 90 km.

relating to photochemistry and energetics. A summary concludes the paper.

2. Measurement and Retrieval Approach

[5] SABER continually measures emission from the Earth's limb by scanning from 400 km tangent altitude down to the hard Earth surface. Shown in Figure 1 (left) is an example of a single daytime limb radiance measurement scan. The dashed line in the figure is the noise equivalent radiance (2.4×10^{-10} W cm^{-2} sr^{-1}) in the SABER $O_2(^1\Delta)$ channel. SABER is a filter radiometer and the nominal 5% transmission points are 7703 to 7971 wave numbers (1.298 μm to 1.254 μm). The figure illustrates the large signal-to-noise (S/N) available in the SABER $O_2(^1\Delta)$ measurement, i.e., a S/N exceeding 1000 below 90 km tangent altitude.

[6] The measured limb radiance R is described by the radiative transfer equation:

$$R = \int J_\nu(x)\phi_\nu \frac{\partial \tau_\nu(x)}{\partial x} dx\, d\nu \qquad (1)$$

where $J_\nu(x)$ is the source function at wave number ν at location x along the line of sight, ϕ_ν is the SABER relative spectral response function at wave number ν, and $\partial\tau_\nu(x)/\partial x$ is the gradient of transmission (τ_ν) at wave number ν at location x along the line of sight. Below 65 km the emission is self absorbed, while above the emission is in the weak-line radiative transfer limit.

[7] The first products to be derived from the limb radiance are the volume emission rates V_e (erg cm^{-3} s^{-1}) of energy and V_p (photons cm^{-3} s^{-1}) of 1.27 μm photons ($V_p = V_e/hc\nu$, h is Planck's constant and c is the speed of light.) The emission rates are derived above 70 km from an Abel (weak-line) inversion of the limb radiance. This process yields the volume emission rate as weighted by the SABER relative spectral response function. To obtain the total, unweighted emission rate, a correction factor is applied to the derived weighted emission rate. This process of "unfiltering" the emission rate in the weak line limit is described by *Mlynczak et al.* [2005]. For the SABER $O_2(^1\Delta)$ emission the factor is about 1.28. That is, the total $O_2(^1\Delta)$ emission rate is approximately 1.28 times the weighted emission rate. The "unfilter" factor has a weak dependence on temperature as the relative strengths of the spectral lines change with temperature. This weak (4% maximum) effect is accounted for in the volume emission rate retrieval using SABER-measured temperatures (also from version 1.07 of the data set).

[8] Below 70 km absorption of the $O_2(^1\Delta)$ emission by O_2 itself begins to become important and the weak-line retrieval approach becomes invalid. At these altitudes the volume emission rates are derived by inverting equation (1) to obtain the source function for the $O_2(^1\Delta) \rightarrow O_2(^3\Sigma)$

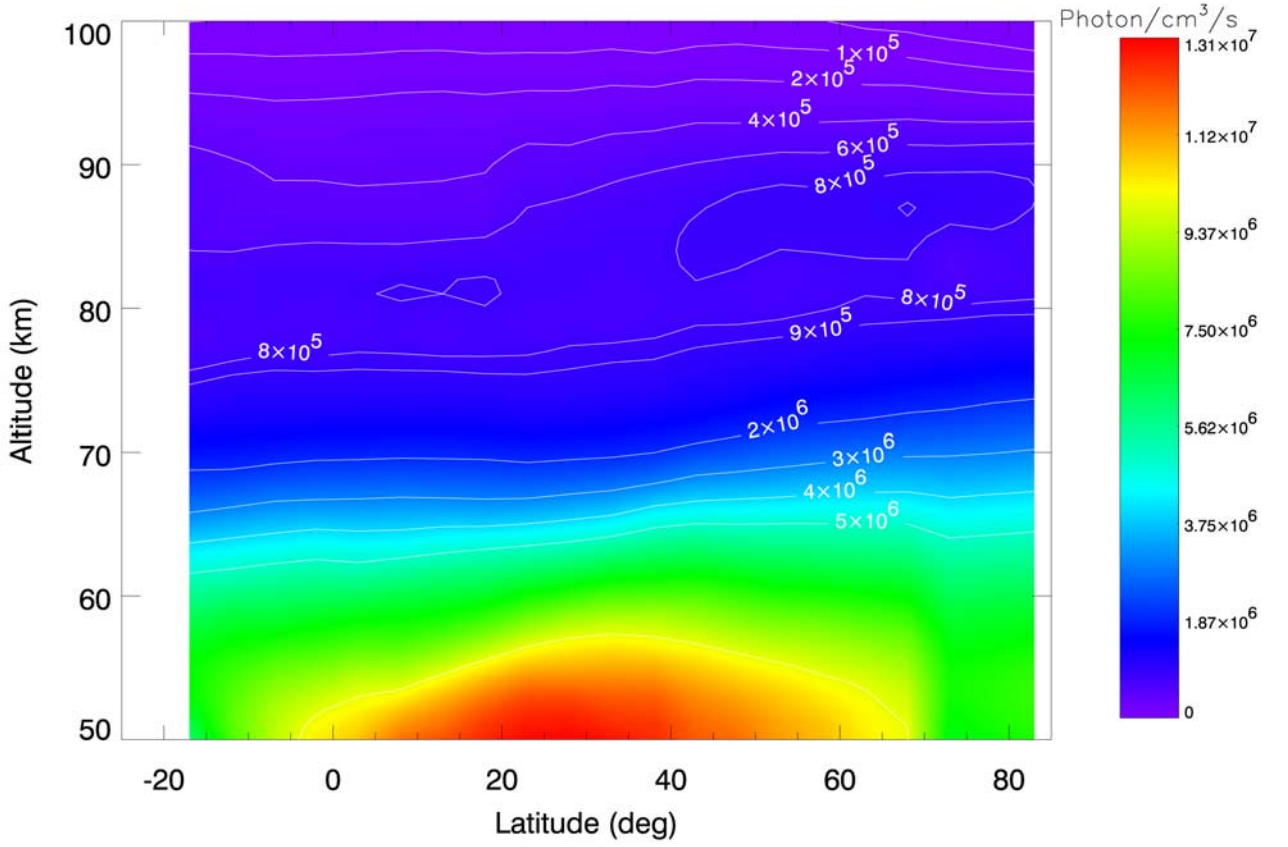

Figure 2. Daytime $O_2(^1\Delta)$ zonally averaged photon volume emission rate for day 185 in 2002.

transition. This process is straightforward as the O_2 density that determines the transmittance gradient is known from the SABER temperature and pressure retrieval, assuming an O_2 mixing ratio of 0.21. The radiative transfer equation is evaluated in the strong line regime using the BANDPAK software library [*Marshall et al.*, 1994], updated for non-LTE conditions [*Mlynczak et al.*, 1994]. The volume emission rate V_p is derived from the source function through the relationship

$$V_p = \frac{4\pi}{hc\nu} J \frac{\partial \varepsilon}{\partial x} \tag{2}$$

where J is the retrieved, spectrally integrated source function, and $\partial\varepsilon/\partial$x is the gradient of emissivity at the tangent point. The weak line and strong-line retrievals are blended together to achieve a single volume emission rate profile, an example of which is shown in Figure 1 (right) for the radiance profile shown in Figure 1 (left). The noise equivalent volume emission rate is about 600 photons cm^{-3} s^{-1} as indicated by the dashed line.

3. Results

3.1. Odd-Oxygen Chemistry

[9] Figure 2 shows the volume emission rate of photons, V_p, on day 185 (4 July) from year 2002. The data in the figure are zonal averages in 5° latitude bins taken for all the daytime orbits, i.e., for solar zenith angles less than 85°. In all the succeeding figures the data are averaged this way and are referred to as zonal averages. The emission rates range from approximately 1×10^5 photons cm^{-3} s^{-1} to over 1×10^7 photons cm^{-3} s^{-1}. From these rates we can first illustrate just how far the $O_2(^1\Delta) \rightarrow O_2(^3\Sigma)$ transition is from local thermodynamic equilibrium (LTE). The transition temperature (T_t) can be defined from the relation:

$$\frac{n_u}{n_0} = \frac{g_u}{g_0} \exp(-E/k_b T_t) \tag{3}$$

where n_u is the upper ($O_2(^1\Delta)$) state population, n_0 the lower ($^3\Sigma$) state population, E is the energy of a 1.27 μm photon, and k_b is Boltzmann's constant. The degeneracies are taken from *Mlynczak and Nesbitt* [1995] with $g_u = 2$ and $g_l = 3$. The upper state number density n_u is obtained from the photon volume emission rate by the relation $V_p = n_u A$, where A is the Einstein coefficient for spontaneous emission of the $O_2(^1\Delta)$ to the ground $O_2(^1\Sigma)$ state. The lower state density n_0 is obtained from the O_2 density and is derived from SABER temperature and pressure measurements, using the MSIS model [*Hedin*, 1991] to provide the O_2 mixing ratio. Shown in Figure 3 are the zonally averaged transition temperatures for the 1.27 μm transition in the mesosphere as derived from the SABER $O_2(^1\Delta)$ volume emission rates. They are consistent with those predicted by *Mlynczak et al.* [1994] using ozone abundances from the

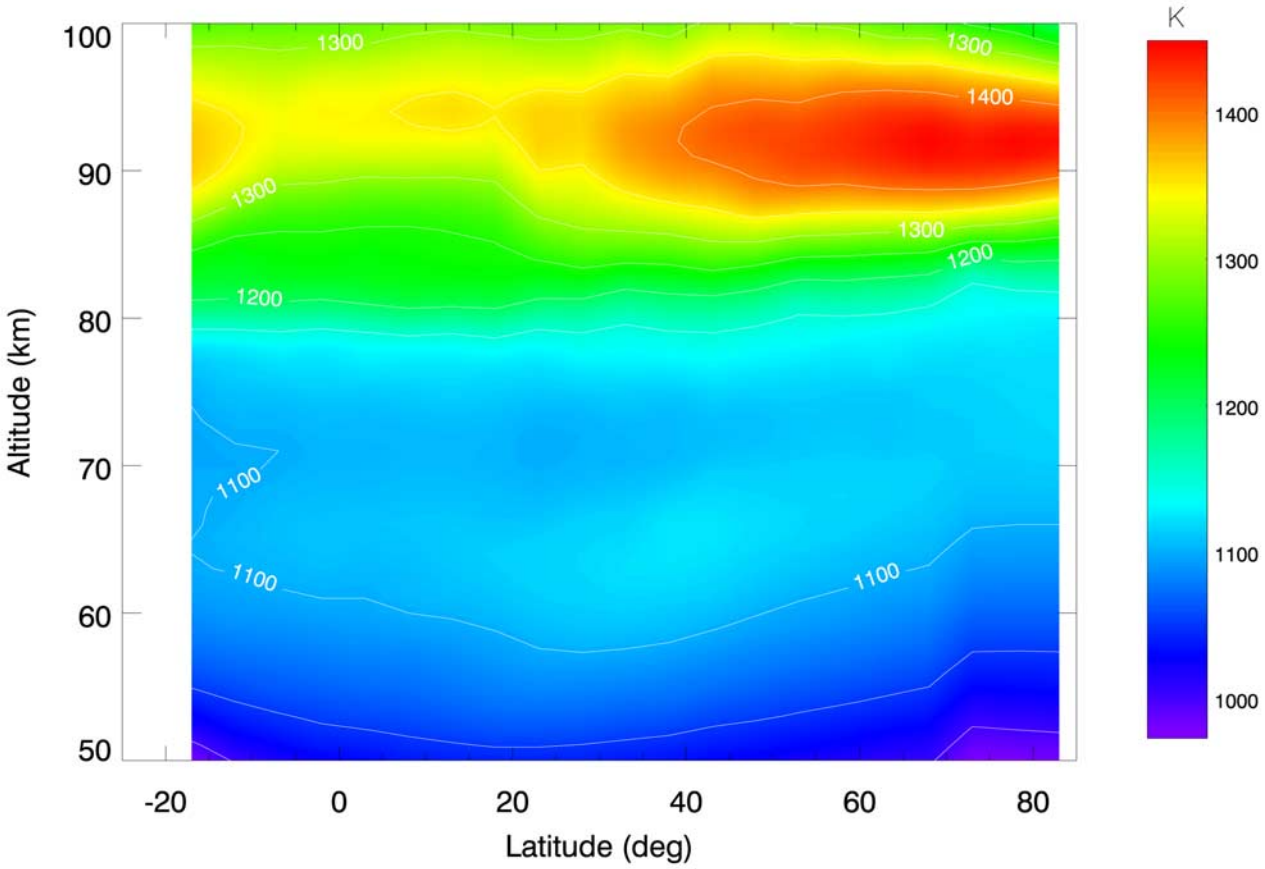

Figure 3. Zonally averaged transition temperatures (K) for the $O_2(^1\Delta) \rightarrow O_2(^3\Sigma)$ transition as derived from SABER.

Garcia-Solomon two-dimensional photochemical model. The transition temperatures range from just over 1000 K near the stratopause to over 1400 K near the cold summer mesopause. As the kinetic temperatures in the mesosphere generally span the range from 270 K to 150 K, the $O_2(^1\Delta) \rightarrow O_2(^3\Sigma)$ state is clearly driven quite far from LTE. In fact, all of the SABER-observed emissions are not in LTE above the stratopause.

[10] The ozone concentration can be inferred from the photon volume emission rate using a non-LTE radiative and kinetic model, as was demonstrated by the SME experiment. The SABER ozone data are derived using the model of *Mlynczak et al.* [1993] with the following updates: (1) The Hartley band solar irradiance used to compute the ozone photolysis rate is taken from the Woods-Rottman solar model [*Woods et al.*, 2000; *Woods and Rottman*, 2002]; (2) the solar irradiance at Lyman-α and in the Schumann-Runge continuum is also taken from the Woods-Rottman model; (3) the radiative lifetime of the $O_2(^1\Delta) \rightarrow O_2(^3\Sigma)$ transition is now 2.23×10^{-4} s^{-1} based on the work by *Lafferty et al.* [1998] and confirmed by *Smith and Newnham* [2000], as opposed to the classic result of 2.58×10^{-4} s^{-1} reported by *Badger et al.* [1965]; (4) solar excitation in the O_2 "B" and "γ" atmospheric bands at 688 and 629 nm are added to the usual atmospheric ("A") band excitation at 762 nm. *Slanger and Copeland* [2003] indicate that at mesospheric densities the process of quenching of the $\upsilon = 2$ and $\upsilon = 1$ levels to the $\upsilon = 0$ level of the $O_2(^1\Sigma)$ state proceeds quite rapidly relative to emission. Solar excitation of the A, B, and γ bands must be included as the $O_2(^1\Sigma)$ state is quenched to the $O_2(^1\Delta)$ state; (5) solar excitation of the $O_2(^1\Delta)$ state itself [*Mlynczak and Marshall*, 1996]; and (6) increased yield of $O_2(^1\Sigma)$ from collisions with $O(^1D)$ [*Green et al.*, 2000] and increased quantum yield of $O(^1D)$ in photolysis of O_2 at Lyman-α wavelengths [*Lacoursiére et al.*, 1999]. These changes are all minor relative to *Mlynczak et al.* [1993], with the exception of the 13.5% decrease in radiative lifetime of the $O_2(^1\Delta)$ state, and are included for completeness.

[11] Shown in Figure 4 are the zonally averaged ozone profiles inferred from the retrieved SABER photon volume emission rates. The data are ozone volume mixing ratios in parts per million by volume and range from 2.4 ppmv in the lower mesosphere (52 km) just above the midlatitude stratopause, through a minimum of 0.2 ppmv throughout the middle mesosphere (70–80 km). The secondary ozone maximum of 2.2 ppmv occurs at about 70°N latitude near 92 km. We note that this secondary maximum occurs in the vicinity of the cold polar summer mesopause. The data in Figure 4 represent a composite of approximately 600 individual daytime ozone profiles recorded on 4 July 2002. Of these, just over 400 were recorded between

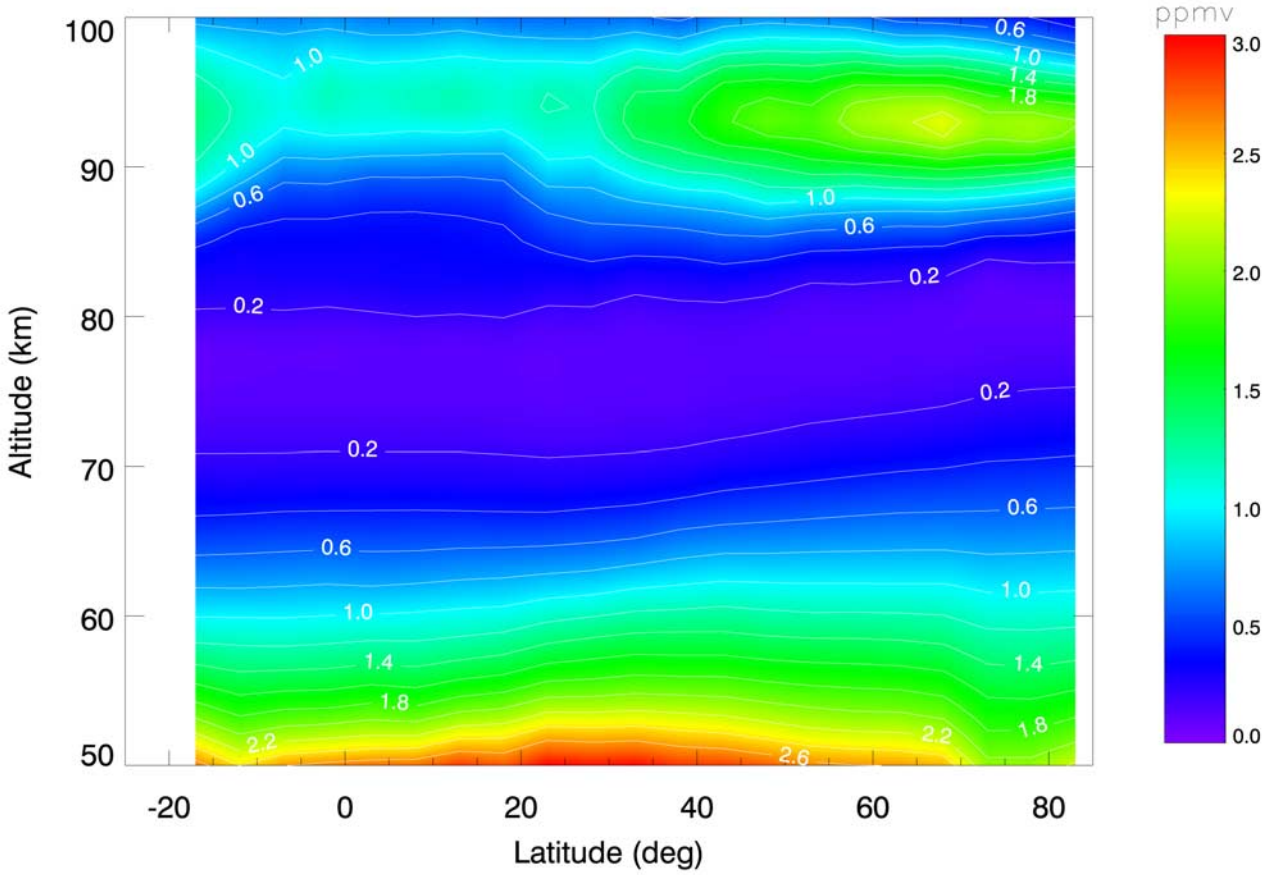

Figure 4. Zonally averaged ozone volume mixing ratios (parts per million) for day 185 year 2002.

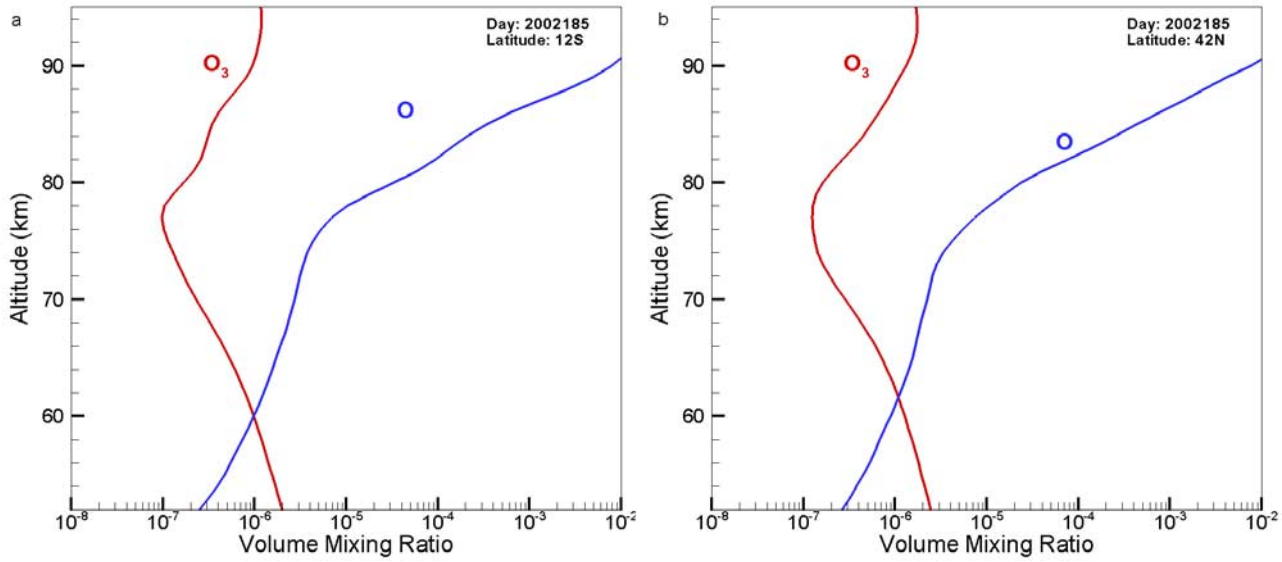

Figure 5. Single ozone profile derived from the $O_2(^1\Delta)$ volume emission rate and the atomic oxygen derived from the ozone under the assumption of photochemical steady state, at (a) 12°S latitude, day 185, year 2002, and (b) 42°N latitude, day 185, year 2002.

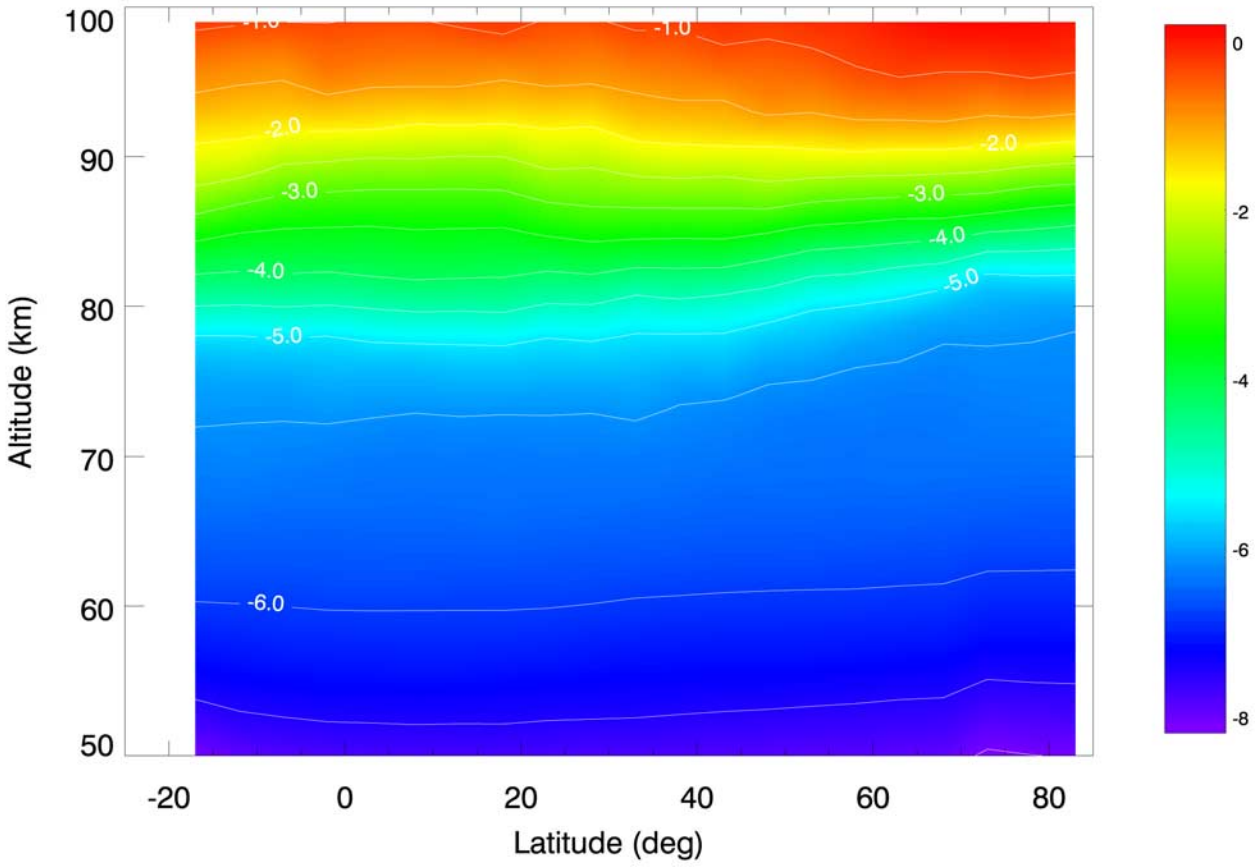

Figure 6. Base 10 logarithm of the zonally averaged atomic oxygen mixing ratio profiles derived from SABER ozone.

1600 and 1700 local time; an additional 100 profiles were recorded in the next 3 hours. The remaining profiles were taken between 2100 and 0200 local time (recall that the data shown here occurs on a day in northern hemisphere polar summer). An assessment of the ozone abundances against photochemical models will require consideration of the variability with local time and solar zenith angle.

[12] During the daytime the lifetime of ozone against photolysis is about 2 min, implying that photochemical steady state is a reasonable assumption to describe the ozone abundance. In the daytime, a SABER data product of atomic oxygen is derived from the ozone based on this assumption. We equate production of ozone by recombination of atomic oxygen and molecular oxygen with destruction of ozone by photolysis to derive the atomic oxygen concentration. Shown in Figures 5a and 5b are plots of the ozone and atomic oxygen mixing ratios at latitudes indicated in the figures. Of particular note is that atomic oxygen is shown to become the dominant odd-oxygen component above about 60 km altitude, which is consistent with daytime photochemical model predictions [*Garcia and Solomon*, 1983]. Atomic oxygen derived in this fashion is also available as a SABER data product in Version 1.07. An example of the zonally averaged atomic oxygen mixing ratios is shown in Figure 6. Because the mixing ratio of atomic oxygen spans a large range we plot the base 10 logarithm of the volume mixing ratio. From Figure 6 we see that the mixing ratio exceeds 1% (10^{-2}) just above 90 km, again consistent with photochemical theory.

3.2. Energetics

[13] As mentioned above, the $O_2(^1\Delta)$ emission is a fundamental component of the radiative energy budget of the mesosphere. Shown in Figure 7 are the zonally averaged energy loss rates (erg cm^{-3} s^{-1}) for this transition derived from the SABER photon volume emission rates. These are the instantaneous rates at which energy is being radiated away locally, substantially reducing the amount of solar energy available for heat. We can illustrate the energy loss by converting the energy loss rates V_e to loss rates Q_l in Kelvin per day, from the first law of thermodynamics ($V_e = \rho\, C_p\, Q_l$),

$$Q_l = \frac{2}{7}\frac{1}{k_b M} V_e \tag{4}$$

where ρ is density, C_p is the heat capacity at constant pressure, and M is the number density derived from SABER temperature and pressure measurements. The factor of 2/7 is due to the relationship between the gas constant and the heat capacity for diatomic molecules. The derivations of Q_l are shown in Figure 8. The maximum energy loss rates occur in

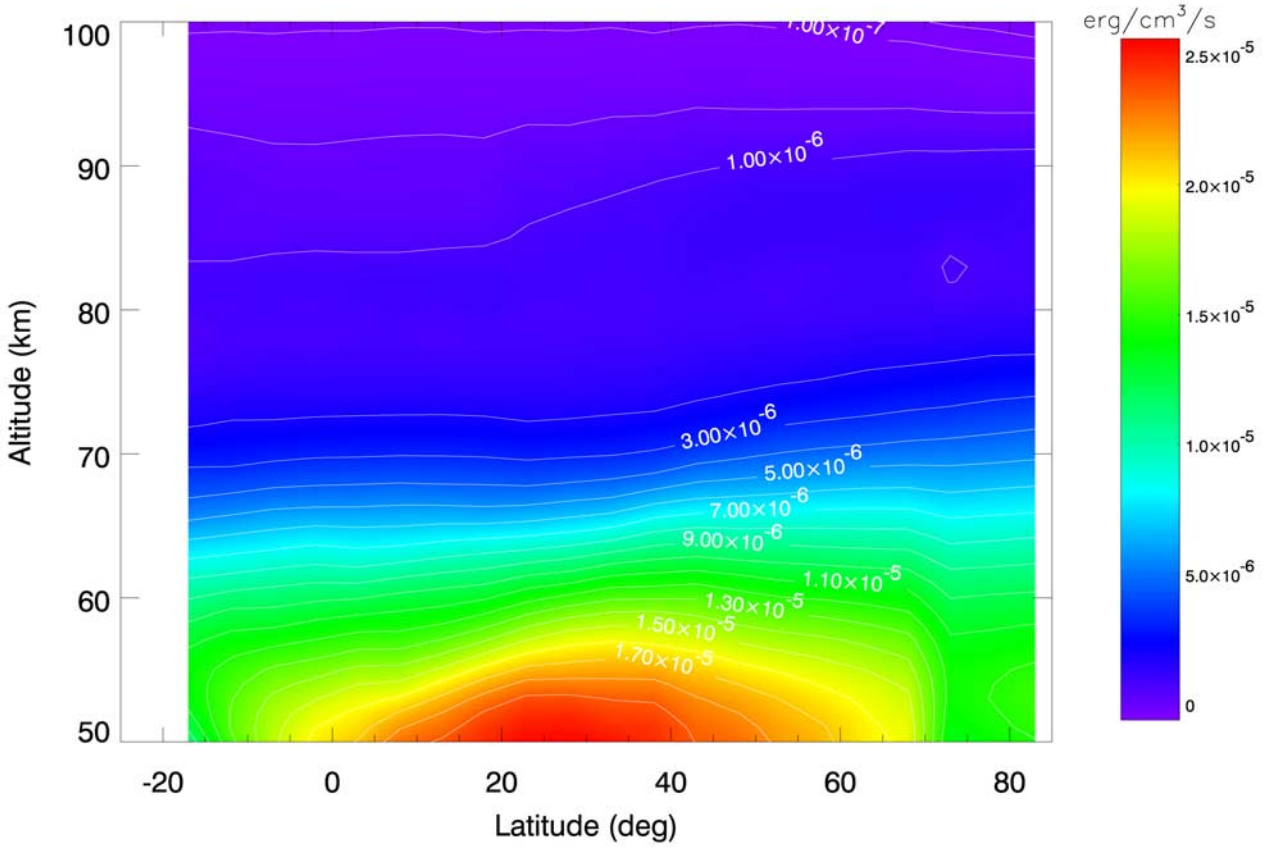

Figure 7. Zonally averaged volume emission rate of energy (erg cm^{-3} s^{-1}) for the $O_2(^1\Delta) \rightarrow O_2(^3\Sigma)$ transition.

the vicinity of the cold summer mesopause on this day, with rates exceeding 3 K/day. The results in Figure 8 can be interpreted as the additional rate at which the atmosphere would be heated if the $O_2(^1\Delta)$ airglow did not occur. However, as shown by *Mlynczak and Solomon* [1991, 1993], the oxygen emission substantially reduces the amount of solar energy available for heat, resulting in heating efficiencies for the ozone Hartley band, O_2 at Lyman-α, and the O_2 Schumann-Runge continuum that are substantially less than unity. Also, using a technique demonstrated by *Mlynczak and Solomon* [1991], the airglow energy loss rates, when combined with the independently derived SABER ozone measured at 9.6 μm, will yield an estimate of the solar heating efficiency of the Hartley band essentially independent of the kinetic and spectroscopic parameters used in the $O_2(^1\Delta)$ airglow model. Heating due to absorption of radiation in the Hartley band of ozone is the main radiative drive for the mesosphere, and the heating efficiencies are fundamental inputs to any dynamical model of the mesosphere.

[14] The $O_2(^1\Delta)$ airglow can also be used to derive the solar energy deposition rate in the ozone Hartley band independent of any knowledge of the ozone abundance and the solar irradiance, as shown by *Mlynczak* [1999]. This approach is applied in the SABER operational data processing system to derive the instantaneous rate of solar energy deposition in the Hartley band. For day 185 of 2002 the zonally averaged energy deposition rates are shown in Figure 9. The rates shown are in Kelvin per day and represent the instantaneous rate at which ozone is absorbing ultraviolet radiation from the Sun in the Hartley band. The rates peak in the lower mesosphere at midlatitudes just above the stratopause at ~25 K/day. As is evident in Figure 9, the rates follow the distribution of ozone as the rate is directly proportional to the product of the photolysis rate and the ozone abundance, and the photolysis rate is essentially constant with altitude in the mesosphere. At the secondary maximum just above 90 km the energy deposition rate exceeds 18 K/day.

[15] We note that the actual rate at which the atmosphere is heated is less than the energy deposition rates shown in Figure 9 for two reasons. First, as discussed by *Mlynczak and Solomon* [1991, 1993], the energy immediately available for heat is less than the energy being deposited, because energy is used to break the O-O_2 bond of ozone. This bond energy is only realized upon a subsequent exothermic chemical reaction which may occur some time and some distance away from the location of the original solar energy deposition. Second, the airglow reduces the amount of energy available for heat. A heating efficiency [e.g., *Mlynczak and Solomon*, 1993] is required to account for the effects of airglow loss. The actual heating rates are

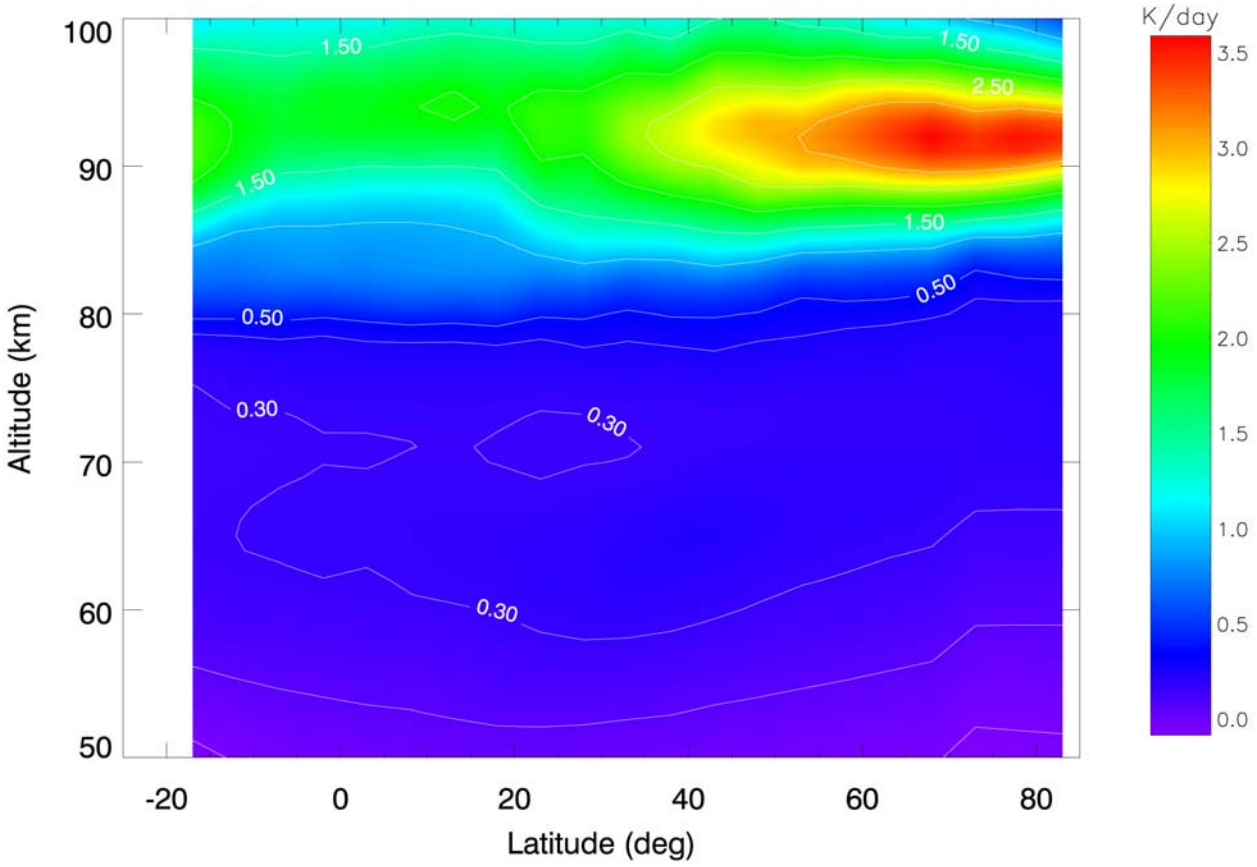

Figure 8. Zonally averaged energy loss rate in Kelvin per day derived from loss rates in Figure 7 through the application of the first law of thermodynamics.

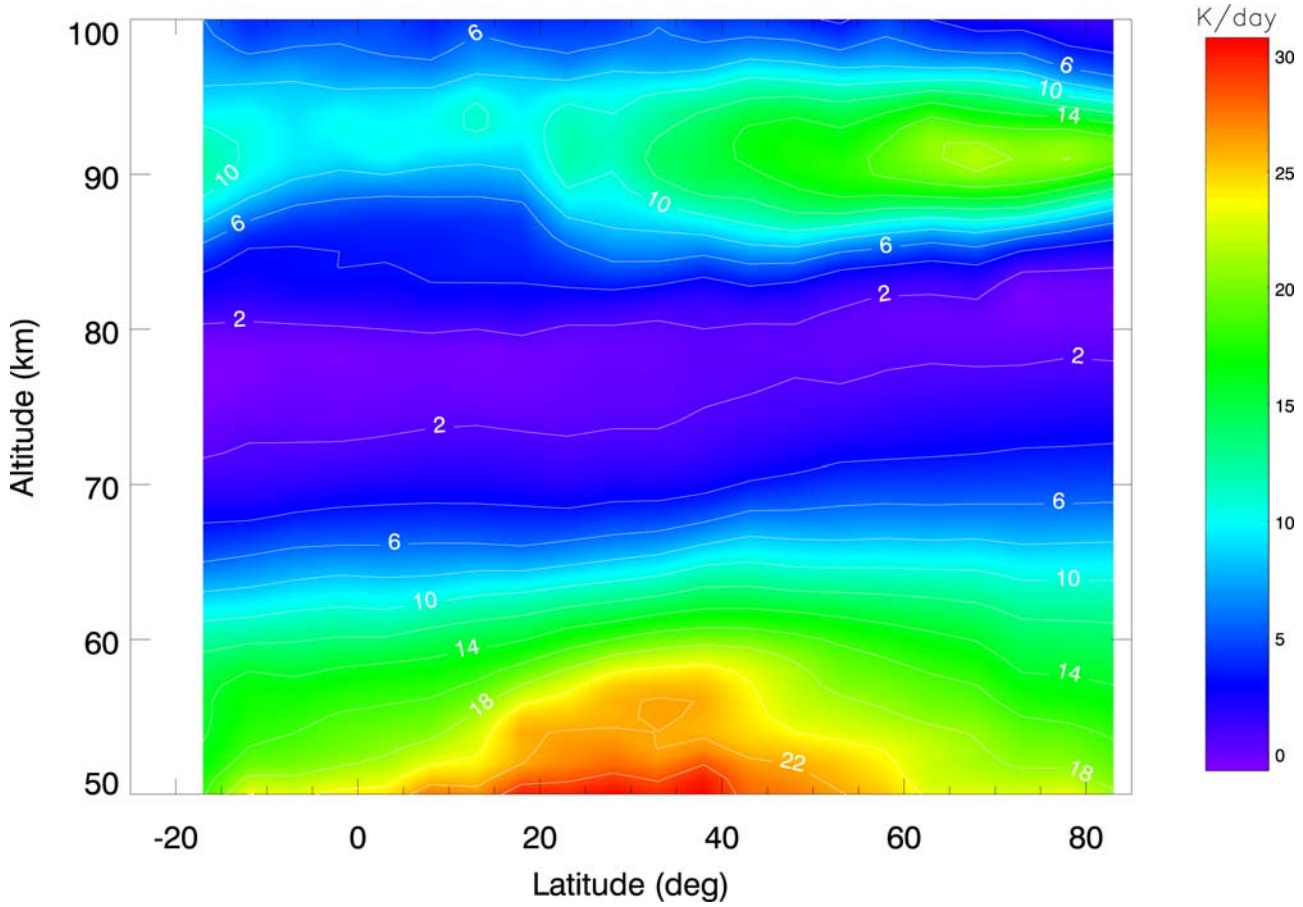

Figure 9. Zonally averaged solar energy deposition rates (K/day) in the Hartley band of ozone derived from the $O_2(^1\Delta)$ airglow, independent of the ozone abundance and solar irradiance, after *Mlynczak* [1999].

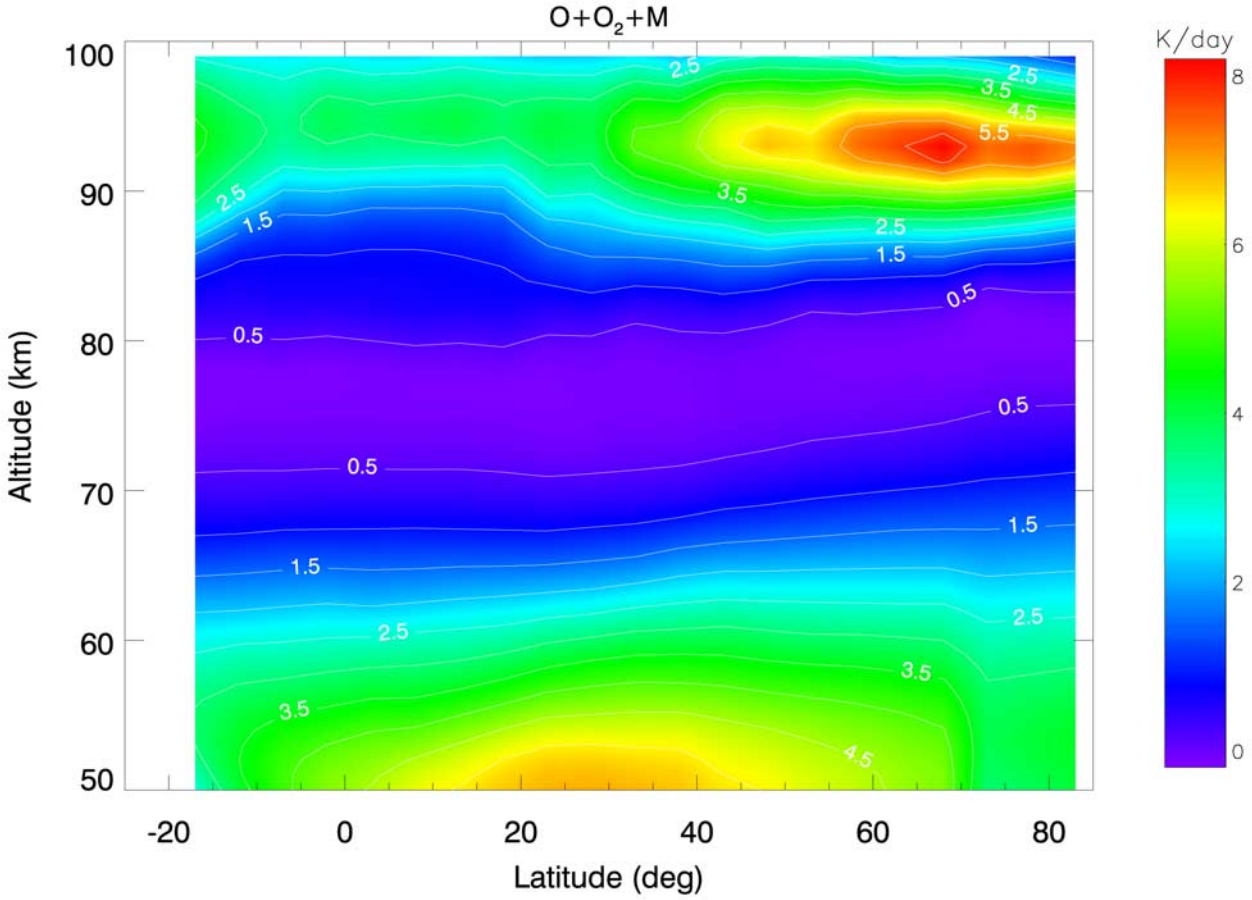

Figure 10. Zonally averaged rates of energy deposition due to the exothermic recombination of $O + O_2 + M \rightarrow O_3 + M$.

readily derived from the SABER energy deposition rates when the bond energy and heating efficiency are taken into account.

[16] Last, the atomic oxygen data may be used along with the SABER temperature and pressure data to derive the rates of heating due to exothermic chemical reactions. In Figure 10 we show the instantaneous, zonally averaged rate of energy deposition due to the recombination of atomic oxygen and molecular oxygen, in Kelvin per day. This component of the chemical heating budget is substantial throughout the entire mesosphere, with rates approaching 5 K/day at the stratopause and 6 K/day near the cold summer mesopause.

4. Summary

[17] We have presented measurements of the $O_2(^1\Delta)$ airglow made by the SABER instrument on the TIMED satellite. From these measurements we are able to infer or derive a variety of parameters related to the odd-oxygen photochemistry and energy budget of the mesosphere and lower thermosphere. The data presented herein are processed with the SABER Version 1.07 algorithms and are now publicly available. The data include the volume emission rates of energy, ozone and atomic oxygen concentrations, and the rates of solar and chemical energy deposition. These data are part of a larger set of SABER data that can be used to study the structure and energy balance of the mesosphere and lower thermosphere. Subsequent publications will describe the retrieval algorithms in greater detail. The SABER $O_2(^1\Delta)$ airglow algorithms presented here will continue to be improved as new processes come to light and as additional processes are evaluated, such as the airglow emission due to O-atom recombination [e.g., *Evans et al.*, 1988].

[18] **Acknowledgments.** The authors thank the NASA Science Mission Directorate for the continued support of the TIMED mission. M.G.M. thanks the Science Directorate at NASA Langley for continued support. The authors also thank A. Smith and D. Marsh of NCAR for constructive comments on the manuscript.

References

Badger, R. M., A. C. Wraight, and R. F. Whitlock (1965), Absolute intensities of the discrete and continuous absorption bands of oxygen gas at 1.26 and 1.065 μm and the radiative lifetime of the $^1\Delta_g$ state of oxygen, *J. Chem. Phys.*, *43*, 4345–4350.

Evans, W. F. J., D. M. Hunten, E. J. Llewellyn, and A. Vallance-Jones (1968), Altitude profile of the infrared atmospheric system of oxygen in the dayglow, *J. Geophys. Res.*, *73*, 2885–2896.

Evans, W. F. J., I. C. McDade, J. Yuen, and E. J. Llewellyn (1988), A rocket measurement of the O_2 infrared atmospheric (0-0) band emission in the dayglow and a determination of the mesospheric ozone and atomic oxygen densities, *Can. J. Phys.*, *66*, 941–946.

Garcia, R. R., and S. Solomon (1983), A numerical model of the zonally averaged dynamical and chemical structure of the middle atmosphere, *J. Geophys. Res.*, *88*, 1379–1400.

Green, J. G., J. Shi, and J. R. Barker (2000), Photochemical kinetics of vibrationally excited ozone produced in the 248 nm photolysis of O_2/O_3 mixtures, *J. Chem. Phys.*, *104*, 6218–6226.

Hedin, A. E. (1991), Extension of the MSIS thermosphere model into the middle and lower atmosphere, *J. Geophys. Res.*, *96*(A2), 1159–1172.

Lacoursiére, J., S. A. Meyer, G. W. Faris, T. G. Slanger, B. R. Lewis, and S. T. Gibson (1999), The O(^{1}D) yield of O_2 photodissociation near H Lyman-α (121.6 nm), *J. Chem. Phys.*, *110*, 1949–1958.

Lafferty, W. J., A. M. Solodov, C. L. Lugez, and G. T. Fraser (1998), Rotational line strengths and self-pressure broadening coefficients for the 1.27 μm $a^1\Delta_g \leftarrow X^3\Sigma_g$ 0-0 band of O_2, *Appl. Opt.*, *37*, 2264–2270.

Llewellyn, E. J., et al. (2004), The OSIRIS instrument on the Odin spacecraft, *Can. J. Phys.*, *82*, 411–422, doi:10.1139/P04-005.

Marshall, B. T., L. L. Gordley, and D. A. Chu (1994), Bandpak: Algorithms for modeling broadband transmission and radiance, *J. Quant. Spectrosc. Radiat. Transfer*, *52*, 581–599.

Mlynczak, M. G. (1997), Energetics of the mesosphere and lower thermosphere and the SABER experiment, *Adv. Space. Res.*, *20*, 1177–1183.

Mlynczak, M. G. (1999), A new perspective on the molecular oxygen and hydroxyl airglows, *J. Geophys. Res.*, *104*, 27,535–27,543.

Mlynczak, M. G., and B. T. Marshall (1996), A reexamination of the role of the A, B, and γ bands in the middle atmosphere heat budget, *Geophys. Res. Lett.*, *23*, 657–660.

Mlynczak, M. G., and D. J. Nesbitt (1995), The Einstein coefficient for spontaneous emission of the $O_2(a^1\Delta_g)$ state, *Geophys. Res. Lett.*, *22*, 1381–1384.

Mlynczak, M. G., and S. Solomon (1991), On the efficiency of solar heating in the middle atmosphere, *Geophys. Res. Lett.*, *18*, 1201–1204.

Mlynczak, M. G., and S. Solomon (1993), A detailed evaluation of the heating efficiency in the middle atmosphere, *J. Geophys. Res.*, *98*, 10,517–10,542.

Mlynczak, M. G., S. Solomon, and D. S. Zaras (1993), An updated model for $O_2(a^1\Delta_g)$ concentrations in the mesosphere and lower thermosphere and implications for remote sensing of ozone at 1.27 μm, *J. Geophys. Res.*, *98*, 18,639–18,648.

Mlynczak, M. G., D. S. Zaras, and M. Lopez-Puertas (1994), Rapid computation of spectrally integrated non-LTE limb emission, *J. Geophys. Res.*, *99*, 25,761–25,772.

Mlynczak, M. G., F. Morgan, J.-H. Yee, P. J. Espy, D. Murtagh, B. Marshall, and F. J. Schmidlin (2001), First simultaneous measurements of the $O_2(^1\Delta)$ and $O_2(^1\Sigma)$ airglows in the daytime mesosphere, *Geophys. Res. Lett.*, *28*, 999–1002.

Mlynczak, M. G., et al. (2005), Energy transport in the thermosphere during the solar storms of April 2002, *J. Geophys. Res.*, *110*, A12S25, doi:10.1029/2005JA011141.

Russell, J. M., M. G. Mlynczak, L. L. Gordley, J. Tansock, and R. Esplin (1999), An overview of the SABER experiment and preliminary calibration results, *Proc. SPIE Int. Soc. Opt. Eng.*, *3756*, 277–288.

Slanger, T. G., and R. A. Copeland (2003), Energetic oxygen in the upper atmosphere and in the laboratory, *Chem. Rev.*, *103*, 4731–4765.

Smith, K. M., and D. A. Newnham (2000), Near-infrared absorption cross sections and integrated absorption intensities of molecular oxygen (O_2, O_2-O_2, and O_2-N_2), *J. Geophys. Res.*, *105*(D6), 7383–7396.

Thomas, R. J., C. A. Barth, D. W. Rusch, and R. W. Sanders (1984), Solar mesosphere explorer near-infrared spectrometer: Measurements of 1.27-μm emission and the inference of mesospheric ozone, *J. Geophys. Res.*, *89*, 9569–9580.

Woods, T., and G. Rottman (2002), Solar ultraviolet variability over time periods of aeronomic interest, in *Atmospheres in the Solar System: Comparative Aeronomy*, *Geophys. Monogr. Ser.*, vol. 130, edited by M. Mendillo, A. Nagy, and J. Hunter Waite Jr., pp. 221–234, AGU, Washington, D. C.

Woods, T. N., W. K. Tobiska, G. J. Rottman, and J. R. Worden (2000), Improved solar Lyman-alpha irradiance modeling from 1947 through 1999 based on UARS observations, *J. Geophys. Res.*, *105*, 27,195–27,215.

L. L. Gordley, B. T. Marshall, and R. E. Thompson, G&A Technical Software, 11864 Canon Boulevard, Suite 101, Newport News, VA 23606, USA.

F. J. Martin-Torres, Analytical Services and Materials, Inc., 107 Research Drive, Hampton, VA 23666, USA.

M. G. Mlynczak and E. E. Remsberg, NASA Langley Research Center, Hampton, VA 23681, USA. (martin.g.mlynczak@nasa.gov)

J. M. Russell III, Department of Atmospheric and Planetary Sciences, Hampton University, Hampton, VA 23668, USA.